Near Surface Geophysics

EAGE EUROPEAN ASSOCIATION OF GEOSCIENTISTS & ENGINEERS

Near Surface Geophysics, 2019, **17**, 581–594 doi: 10.1002/nsg.12071

Permeability estimation from induced polarization: an evaluation of geophysical length scales using an effective hydraulic radius concept

Andreas Weller[1]* and Lee Slater[2]

[1]*Institut für Geophysik, Technische Universität Clausthal, 38678, Clausthal-Zellerfeld, Germany, and* [2]*Department of Earth and Environmental Sciences, Rutgers-Newark, New Jersey, NJ 07102, USA*

Received April 2019, revision accepted September 2019

ABSTRACT

Geophysical length scales defined from induced-polarization measurements can be used in models of permeability (k) prediction. We explore the relative merit of different induced-polarization parameters as proxies of an effective hydraulic radius (r_{eff}) that can be used to predict permeability from a modified Hagen–Poiseuille equation. Whereas geometrical measures of the hydraulic radius are good proxies of r_{eff}, the induced-polarization measures are not well correlated with r_{eff}. However, a new proxy of r_{eff} that considers both imaginary conductivity and formation factor shows an improved correlation with r_{eff}. The resulting model enables a better quality of permeability prediction compared with the other geophysical length scales, but does not reach the predictive quality of the models based on geometrical length scales. The specific polarizability defined when incorporating the effect of the formation factor on imaginary conductivity appears to be independent of pore geometry, indicating that it is the correct parameter representing the role of the surface electrochemistry on the induced-polarization effect. However, the joint dependence of induced-polarization measurements on both the pore radius and the tortuosity and porosity of the interconnected pore network is a limitation to the widely explored use of induced-polarization measurements to isolate surface properties from volumetric properties of the interconnected pore network.

Key words: Complex conductivity, Hydrogeophysics, Induced polarization, Permeability, Porosity.

INTRODUCTION

Induced polarization (IP) is an electrical geophysical prospecting method that records the space charge polarization of ions in the electrical double layer (EDL) forming at the grain–fluid interface. The measurements have proven sensitivity to the pore geometry controlling fluid flow (e.g. Scott and Barker 2003; Weller *et al.* 2010b). Induced-polarization parameters can be interpreted as geophysical length scales that represent proxies of the geometric length scales (e.g. a pore radius) required in permeability (k) prediction models (Robinson *et al.* 2018). A geophysical approach to k estimation could substantially advance subsurface characterization by providing spatially dense information on the distribution of relatively high versus relatively low permeability units. Realizing this goal requires that the geophysical (IP) length scales provide robust proxies of geometric length scales and result in reliable permeability prediction equations.

Geophysical length scales have been defined from two pieces of information extractable from IP data sets: (1) a measure of the dominant relaxation time of the polarization, which is closely related to the dominant pore size of the porous network controlling fluid flow in soil/rock (e.g. Scott and Barker 2003) and (2) a measure of the total strength of the polarization, which is closely related to the total interfacial surface area of the interconnected pore space (e.g. Weller *et al.* 2010b). Beyond an estimated length scale, permeability

*E-mail: andreas.weller@tu-clausthal.de

prediction models also depend on the porosity (ϕ) and tortuosity (T) of the interconnected pore network. These factors are conveniently represented by the electrical formation factor ($F = T/\phi$) that can also be estimated from IP measurements when the fluid conductivity (σ_w) is known (Börner, Schopper and Weller 1996; Weller, Slater and Nordsiek 2013).

The search for robust, IP-derived geophysical length scales has identified discrepancies in the form of the k prediction equations for unconsolidated sediments versus consolidated sedimentary rocks (primarily sandstones). Weller *et al.* (2015) demonstrated, from an empirical perspective, that IP-based k prediction for unconsolidated sediments was mostly controlled by the length scale. In contrast, IP-based k prediction for consolidated sediments foremost depended on the formation factor. The high sensitivity of the k estimate to F in consolidated sedimentary rocks is evidenced by calibration of empirically derived models on large databases predicting power-law exponents of -3 or smaller on the formation factor (e.g. Rink and Schopper 1974; Weller *et al.* 2015; Öner *et al.* 2016). In contrast, theoretical models based on geometrical length scales, for example, the dominant pore radius (Katz and Thompson 1987), and geophysical length scales (Revil *et al.* 2015) typically predict a power-law exponent of -1 on the formation factor, which is sometimes found to only adequately represent unconsolidated sediments (Weller *et al.* 2015).

In this paper, we further evaluate the merit of the concept of geophysical length scales for k estimation discussed by Robinson *et al.* (2018) through a comparison against an effective hydraulic radius (r_{eff}) that can be directly calculated from the Hagen–Poiseuille equation describing a bundle of capillaries. We apply the approach on an extensive database of consolidated sedimentary rocks. By reevaluating the significance of ϕ and T on the polarization magnitude-based length scale, we arrive at a new geophysical length scale that is more strongly associated with the effective hydraulic radius than the previously proposed length scales. Substituting this length scale into the Hagen–Poiseuille equation results in theoretical exponents on F that closely match the observations. We discuss the implications of this study for the reliable estimation of k in sandstones from field-scale measurements of IP.

THEORY

Numerous theoretical approaches to the estimation of the permeability of soils and rocks have been developed with varying degrees of complexity. One relatively simple approach is to combine geometric constraints from a capillary bundle model for fluid flow with the Hagen–Poiseuille equation, which originally describes the flow in a cylindrical tube. The capillary bundle model considers the fluid flow through a larger number of cylindrical capillaries with uniform radius r. Permeability k can then be related to the pore network geometric quantities porosity ϕ, pore radius r and tortuosity T according to the following equation (Pape, Clauser and Iffland 1999):

$$k = \frac{r^2\phi}{8T} = \frac{r^2}{8F}, \tag{1}$$

where the third expression assumes that the electric tortuosity is equal to the hydraulic tortuosity. When permeability and formation factor measurements of samples with varying pore radii are available, equation (1) can be applied to calculate an effective hydraulic radius r_{eff} of a porous medium (Weller *et al.* 2016):

$$r_{\text{eff}} = \sqrt{8Fk}. \tag{2}$$

The effective hydraulic radius needed to predict k is not directly measurable. Consequently, application of equation (1) for k prediction relies on the identification of measurable length scales that represent proxies of r_{eff}. A commonly accepted measurable geometrical proxy of r_{eff} is the dominant pore size r_{dom} that corresponds to the radius of maximum incremental mercury intrusion determined from a Mercury Injection Capillary Pressure (MICP) measurement. A second measurable geometrical property serving as a proxy of r_{eff} results directly from the capillary bundle model, which, for cylindrical capillaries, gives

$$r_{\text{Spor}} = 2/S_{\text{por}}, \tag{3}$$

where S_{por} is the pore volume normalized specific surface area of the bundle. In the case of a real soil or rock sample, S_{por} can be determined from gas adsorption methods (BET method according to Brunauer, Emmett and Teller 1938).

One major limitation of these measurable geometrical proxies of r_{eff} is that both r_{dom} and r_{Spor} are determined from laboratory-scale measurements that provide no solution to the challenge of permeability estimation *in situ* from measurements made either at the surface or in boreholes. Geophysical length scales determined from induced polarization provide a possible solution to this problem (Robinson *et al.* 2018).

The induced-polarization method considers the frequency-dependent complex electrical conductivity (σ^*) of porous media. The real part of σ^* (σ') describes electromigration of the charge carriers and occurs via the electrolyte in the interconnected pore network and ions that make up the electrical double layer at the surface of the pore walls. These

conduction pathways are usually assumed to add in parallel such that

$$\sigma'(\omega) = \frac{1}{F}\sigma_w + \sigma'_{\text{surf}}(\omega), \tag{4}$$

where ω is the angular frequency, σ_w is the conductivity of the pore-filling electrolyte and $\sigma'_{\text{surf}}(\omega)$ is the real part of the complex surface conductivity ($\sigma^*_{\text{surf}}(\omega)$) describing charge transport in the double layer. The imaginary part of $\sigma^*(\omega)$ ($\sigma''(\omega)$) describes temporary charge storage (polarization) that is assumed to exclusively result from counterions in the EDL:

$$\sigma''(\omega) = \sigma''_{\text{surf}}(\omega). \tag{5}$$

Both real and imaginary parts of the complex surface conductivity are frequency (ω) dependent. The polarization strength is represented by the imaginary part of conductivity ($\sigma''(\omega)$). For many samples, a peak in $\sigma''(\omega)$ occurs at a characteristic frequency $f_{pc} = 1/(2\pi\tau_{pc})$, where τ_{pc} is a characteristic relaxation time that depends on the distance over which the charges are displaced during charge storage.

Two types of length scales can be derived from induced polarization using measures of (1) τ_{pc} when measurements are acquired over a sufficiently broad frequency range and (2) polarization magnitude (e.g. $\sigma''(\omega)$). One polarization magnitude-based length scale follows from the empirically derived approximately linear relationship between σ'' and S_{por} (Weller *et al.* 2010b):

$$\sigma'' = c_p S_{\text{por}}, \tag{6}$$

where c_p is the specific polarizability that is assumed to account for the effect of the interfacial chemistry on the polarization magnitude independent of pore geometry. Using the relationship between pore radius and S_{por} for a capillary bundle equation (3) yields the following geophysical length scale:

$$r_{\sigma''} = \frac{2c_p}{\sigma''}. \tag{7}$$

Weller *et al.* (2010b) found that a single value of c_p equal to 10×10^{-12} S adequately described 114 saturated sandstone samples characterized by a narrow range of σ_w variation (0.06–0.114 S/m) when σ'' was measured at 1 Hz. In general, c_p will vary with both σ_w and the surface mineralogy (Weller *et al.* 2011).

Weller and Slater (2012) describe mechanistic models for induced-polarization measurements based either on a diffuse layer polarization model (derived from a surface conductivity expression from Rink and Schopper 1974) or on an extensively used Stern layer polarization (SLP) model (Leroy *et al.* 2008; Revil and Florsch 2010; Revil and Skold 2011). Both models predict that σ'' should also depend on the porosity and tortuosity of the interconnected pore space in addition to S_{por},

$$\sigma'' = c_q \frac{S_{\text{por}}}{F} = c_q \frac{S_{\text{por}}\phi}{T} = c_q \frac{S_m \rho_s (1-\phi)}{T} = c_q \frac{S_m \rho_s (1-\phi)}{\phi F}, \tag{8}$$

where c_q represents a revised definition of the specific polarizability that accounts for the predicted role of F on σ'' ($c_q = \sigma'' F / S_{\text{por}}$), S_m is the specific surface area per unit mass and ρ_s is the grain density. Experimental evidence for $\sigma'' \propto S_{\text{por}}/F$ was demonstrated by Niu *et al.* (2016), who showed that the role of F becomes important in low porosity rocks characterized by high formation factors whereas the relationship shown in equation (6) holds well for higher porosity sandstones. Substituting equation (3) into equation (8) yields another geophysical length scale:

$$r_{F\sigma''} = \frac{2c_q}{F\sigma''}. \tag{9}$$

The geophysical length scale that results from the characteristic relaxation time (τ_{pc}) is (Robinson *et al.* 2018)

$$r_t = \sqrt{2D_+\tau_{pc}}, \tag{10}$$

where D_+ (m^2/s) is a diffusion coefficient for the ions at the mineral–fluid interface involved in the polarization. In the most commonly applied SLP model, the diffusion coefficient is related to the effective ionic mobility β^S_+, temperature T_b, the Boltzmann's constant k_b and the charge of counter ions in the Stern layer q_+ by the Nernst–Einstein relationship $D_+ = k_b T_b \beta^s_+ / |q_+|$. Revil, Koch and Holliger (2012) proposed that r_t is equivalent to the dynamically interconnected pore diameter (Λ) used in the popular Katz and Thompson (1987) permeability model that is derived from percolation theory.

Equations (3), (7) and (10) all define length scales that have been utilized in models of permeability prediction. Whereas r_{Spor} and r_{dom} represent geometric measures of a length scale, $r_{\sigma''}$, $r_{F\sigma''}$ and r_t represent geophysical measures that are limited by being in part controlled by the interfacial chemistry (via c_p, c_q and D_+). Substitutions of r_{dom}, r_{Spor}, $r_{\sigma''}$ and r_t for r_{eff} all result in equations where permeability has a predicted dependence on F^{-1}:

$$k = \frac{a_{\text{dom}}(r_{\text{dom}})^2}{8F}, \tag{11}$$

$$k = \frac{a_{\text{Spor}} r^2_{\text{Spor}}}{8F} = \frac{a_{\text{Spor}}}{2F\left(S_{\text{por}}\right)^2}, \tag{12}$$

$$k = \frac{a_{\sigma''}(r_{\sigma''})^2}{8F} = \frac{a_{\sigma''}(c_p)^2}{2F(\sigma'')^2} \quad (13)$$

and

$$k = \frac{a_t(r_t)^2}{8F} = \frac{a_t D_+ \tau_{pc}}{4F}. \quad (14)$$

The parameters a_{dom}, a_{Spor}, $a_{\sigma''}$ and a_t each represent an empirical fitting parameter based on a presumed linear relationship between r_{eff} and the corresponding measurable geometric proxy (r_{dom}, r_{Spor}) and geophysical proxy ($r_{\sigma''}$, r_t) length scales.

Substitution of the measurable geophysical proxy $r_{F\sigma''}$ for r_{eff} results in an equation where permeability has a predicted dependence on F^{-3},

$$k = \frac{a_{F\sigma''}(r_{F\sigma''})^2}{8F} = \frac{a_{F\sigma''}(c_q)^2}{2F^3(\sigma'')^2}, \quad (15)$$

where $a_{F\sigma''}$ is again an empirical fitting parameter, this time assuming a linear relationship between r_{eff} and $r_{F\sigma''}$. The significance of this stronger influence of F on the permeability prediction from proxy length scales predicted by equation (15) will be explored in this paper.

METHODS

Following the approach taken in previous papers, we utilize a large database of sandstone samples from a variety of independent studies. In all cases, the raw electrical data and physical property measurements are available. This database includes 119 sandstone samples, the majority (109) having been presented in Weller *et al.* (2015, 2016) and Robinson *et al.* (2018). The compilation of samples presented in Weller *et al.* (2015) includes samples from a variety of original sources (Lesmes and Frye 2001; Breede 2006; Schröder 2008; Zhang and Weller 2014). Eleven of the samples in the database appeared in both Weller *et al.* (2015, 2016). Fourteen of the samples in the database appear in both Weller *et al.* (2016) and Robinson *et al.* (2018). Ten new samples have been added to the database, seven being samples from the Baharija Formation (Egypt) and three being samples from the Shahejie Formation (China). The entire database of 119 samples used in this study is presented in Table 1.

The measured geometrical properties include k determined from gas permeametry, ϕ from weight loss on drying and S_m from gas adsorption from which S_{por} was determined. The formation factor was determined either by fitting equation (4) to multi-salinity measurements or from a single measure of σ' made at a sufficiently high σ_w to assume that $\sigma'_{\mathrm{surf}} \ll \sigma_w/F$. The resulting database is characterized by a wide variation in physical properties including ϕ (0.08–0.3), S_{por} (1–185/μm^{-1}), k (1.67E−17 to 4.65E−12 m^2) and F (9–115). In all cases, S_m was acquired on intact (i.e. not crushed) rock samples using the nitrogen BET method. All samples in the database were devoid of obvious indications of significant anisotropy, such as layering, lamination or elongated cracks.

Induced-polarization data were acquired over four or more orders of magnitude of frequency variation for all samples in the database. In each case, the σ^* spectra were obtained by measuring the impedance magnitude and phase shift of the voltage waveform recorded across the sample relative to the current waveform recorded on a reference resistor, the source typically being a sine signal swept over a range of frequencies (e.g. Slater and Lesmes 2002). All measurements reported here were recorded using a four-electrode set-up, whereby separate electrode pairs were used to inject the current into the sample and record the resulting potential waveform across the sample. Measured magnitude and phase shift of the impedance were converted into a complex conductivity (σ^*) using the geometric factor defining the measurement geometry and assuming parallel current flow through the sample in the test device. The majority of samples were saturated with a NaCl solution with $\sigma_w \approx 100$ mS/m. Samples from Robinson *et al.* (2018) were saturated with $\sigma_w \approx 67$ mS/m and required a minor correction to equivalent values of σ'' at 100 mS/m based on the reported weak dependence of σ'' on salinity in metal-free rocks (e.g. Weller *et al.* 2011). As the relaxation time distributions are not significantly controlled by σ_w, no salinity correction for τ_{pc} was necessary.

RESULTS

Geometrical length scales

We first assess how the length scales determined from destructive MICP (r_{dom}) and gas adsorption (r_{Spor}) measurements relate to r_{eff} determined from equation (2). Figure 1(a) shows the log of r_{eff} plotted versus the log of r_{dom}, with samples from the different databases distinguished by different symbols. The 1:1 line is shown (black) along with the best-fitting relation using the function $\log_{10}(r_{\mathrm{eff}}) = \log_{10}(r_{\mathrm{dom}}) + A$ (red) that results in the linear relation $r_{\mathrm{eff}} = 0.414 r_{\mathrm{dom}}$ with a coefficient of determination $R^2 = 0.528$. Figure 1(b) shows the log of r_{eff} plotted versus the log of r_{Spor}. The best-fitting linear relation is determined as $r_{\mathrm{eff}} = 13.0 r_{\mathrm{Spor}}$ ($R^2 = 0.498$). The underestimation of r_{eff} using $r_{\mathrm{Spor}} = 2/S_{\mathrm{por}}$ is expected given the fractal

Table 1 Summary of physical properties for all samples used in this study: specific surface area per unit pore volume (S_{por}), permeability (k), formation factor (F), imaginary part of conductivity measured at 1 Hz and corrected to fluid salinity of 0.1 S/m (σ''), the relaxation time (τ_{pc}), the dominant pore size determined from MICP (r_{dom}) and the effective pore radius (r_{eff}) determined by equation (2)

Sample name	S_{por} (1/μm)	k (in m²)	F	σ'' (mS/m)	τ_{pc} (s)	r_{dom} (μm)	r_{eff} (μm)	Reference†
B-LF	8.30	2.28E−13	16.70	0.0773			5.519	a
GR	31.33	3.30E−13	11.66	0.3034	3.4750	21.140	5.550	a, b
BU3	46.24	2.00E−17	68.35	0.1876	0.8692	0.840	0.105	a, b
BU12	10.46	3.41E−13	17.64	0.0547	0.0068	21.140	6.937	a, b
BK	3.39	1.97E−12	18.22	0.0438			16.964	a
BS4	27.95	4.23E−13	17.84	0.1603			7.774	a
BR5	15.01	4.65E−12	9.04	0.2779	3.4750	21.140	18.329	a, b
BU1	25.35	1.91E−16	38.03	0.3524	0.8692	0.737	0.241	a, b
OK4	8.23	7.39E−15	24.77	0.1183	0.2173	3.345	1.210	a, b
B49H	3.29	6.85E−14	26.82	0.0311			3.835	a
B49V	3.54	4.75E−14	30.98	0.0311			3.430	a
B4H	8.93	3.00E−16	44.94	0.0568			0.328	a
B4V	8.29	2.40E−16	59.56	0.0409			0.338	a
GR1	35.00	1.98E−12	9.41	0.3090	3.4750	18.128	12.206	a, b
AC5	185.34	5.00E−17	115.71	0.1439	0.1592		0.215	a
B4	8.17	2.15E−13	15.19	0.0989	1.1292		5.111	a
BE1	10.73	2.50E−13	21.89	0.0835	0.8480		6.616	a
Co7	61.43	2.63E−15	47.36	0.1836	0.5530		0.998	a
E3	3.93	4.64E−12	14.74	0.0396	1.8000		23.394	a
G4	48.98	5.73E−15	27.06	0.1518	0.9270		1.114	a
IR01	8.84	1.33E−14	37.41	0.0388	1.3220		1.991	a
IR02	8.84	2.23E−14	33.33	0.0367	1.4030		2.440	a
O5	15.71	5.05E−14	17.02	0.1232	0.8550		2.622	a
CLASH		5.23E−13	21.18	0.0878	3.1930		9.415	a
BH6-A2	4.22	4.27E−13	14.05	0.0533	0.1264		6.931	a
ES4-R2	44.11	2.58E−13	16.34	0.3255	1.5915		5.813	a
OK5-R3	11.97	4.12E−14	28.59	0.1226	0.5033		3.069	a
CS-1	48.32	1.29E−16	46.70	0.1409	0.0634	0.176	0.219	b, c
CS-2	17.94	1.83E−14	27.70	0.2573	0.5033		2.013	b
CS-3	12.13	2.51E−14	26.50	0.2039	0.7977	3.679	2.305	b, c
CS-4	3.39	6.05E−14	28.80	0.0954	2.5224		3.734	b
CS-5	7.36	4.57E−14	28.70	0.1098	1.5916	4.898	3.239	b, c
CS-6	97.35	8.08E−17	39.60	0.1380	0.2004		0.160	b
CS-7	113.60	1.30E−16	38.50	0.1489	0.5033		0.200	b
CS-8	114.77	2.27E−16	34.50	0.2028	1.2642		0.250	b
CS-9	142.27	3.64E−16	32.46	0.1209		0.232	0.307	New
CS-10	129.71	4.32E−16	27.20	0.1440			0.307	New
CS-11	65.41	6.24E−16	31.00	0.2828	0.3998	0.735	0.393	a, b
CS-12	64.35	1.30E−15	33.60	0.2870	0.7977		0.590	b
CS-13	19.55	7.05E−15	25.40	0.2692	0.7977	2.454	1.197	a, b
CS-14	20.96	5.96E−15	26.90	0.2194	1.0042	2.726	1.133	b, c
CS-15	44.68	1.88E−15	30.70	0.2528	1.2642		0.679	b
CS-16	9.35	9.01E−15	38.00	0.1651	0.3998	2.887	1.655	a, b
CS-17	14.46	1.09E−14	46.2	0.0834	0.7977		2.009	b
CS-18	4.57	2.37E−14	26.8	0.1068	0.7977	4.201	2.252	b, c
CS-19	56.55	4.30E−17	83.3	0.0843	0.0798		0.169	b
CS-20	6.90	1.43E−14	28.2	0.0818	0.7977		1.795	b
CS-21	11.27	3.59E−15	64.3	0.0630	1.5916		1.359	b

(*Continued*)

Table 1 Continued

Sample name	S_{por} (1/μm)	k (in m²)	F	σ'' (mS/m)	τ_{pc} (s)	r_{dom} (μm)	r_{eff} (μm)	Reference†
CS-22	35.61	4.58E−17	72.3	0.0574	0.5033	0.118	0.163	a, b
CS-23	11.80	2.22E−15	43.0	0.0562	1.0042		0.873	b
CS-25	75.24	1.67E−17	113.6	0.1017			0.123	New
3	39.01	9.60E−17	35.0	0.1383			0.164	New
7H1	2.74	5.13E−14	20.0	0.1312	6.3360	6.520	2.866	b, c
13H1	147.91	5.80E−16	41.0	0.1577			0.436	New
18H1	15.74	1.08E−14	16.0	0.2734	1.2640	3.345	1.176	b, c
22H	37.82	3.57E−15	27.9	0.2682	1.0040	2.583	0.893	b, c
28H1	1.35	6.83E−14	22.1	0.0359	1.5920	4.204	3.472	b, c
28H2	2.70	6.15E−14	18.7	0.0660			3.037	New
31H1	33.77	1.03E−16	34.4	0.1411			0.168	New
43H1	2.49	1.34E−13	12.4	0.1263	2.5220	8.136	3.648	b, c
48H2	115.86	6.37E−17	27.1	0.1181			0.118	New
45	77.99	1.76E−16	62.4	0.0684			0.296	New
49	63.71	1.45E−15	29.5	0.2580			0.584	New
53H1		1.16E−13	19.2	0.0650	2.5224	7.336	4.224	b
53H2	3.89	1.15E−13	13.1	0.1139	2.5220	7.327	3.475	b, c
55	19.66	1.02E−13	14.5	0.3196	0.7980	5.341	3.450	b, c
BE	3.36	5.55E−13	10.8	0.0692	0.3073	14.175	6.934	b
BH6	4.12	4.26E−13	11.9	0.0425		17.860	6.358	b, c
ES-14	1.06	2.88E−12	18.7	0.0939	0.2173	15.874	20.733	b, c
FL	30.50	1.87E−15	34.8	0.2535	3.4768	0.772	0.721	b
IG	4.31	4.52E−13	9.9	0.1144	13.9073	35.996	5.971	b
NS2/2R	165.15	1.37E−15	30.7	0.3342	0.0252	0.329	0.580	b
OK	7.81	1.10E−14	17.0	0.0916	1.2292	0.775	1.221	b
Roett	26.27	3.45E−14	32.7	0.0969	4.0744	4.898	3.003	b
Ska	2.16	4.79E−13	12.7	0.0418	4.0744	14.522	6.976	b
Ud	11.00	8.48E−14	30.7	0.1023	0.5093	9.139	4.566	b
C3-Cl-100.0	47.05	1.89E−15	50.1	0.4782	0.5184	3.281	0.870	c
C3-Cl-118.6	25.69	7.39E−15	38.9	0.4194	0.3235	4.095	1.516	c
C3-Cl-139.7	34.48	1.31E−15	46.5	0.4930	2.1507	2.451	0.698	c
C3-P-015	22.15	4.55E−15	51.0	0.3900	0.0489	3.281	1.362	c
C3-P-019	21.40	3.73E−15	45.1	0.5347	0.1257	3.105	1.160	c
C3-P-021	29.40	7.93E−16	50.8	0.5003	0.0784	1.768	0.568	c
C3-P-022	51.19	2.71E−15	50.9	0.5420	0.0190	6.026	1.050	c
C3-P-023	36.92	4.96E−16	46.6	0.6450	0.0489	2.450	0.430	c
C3-P-024	43.57	1.80E−15	39.7	0.5739	0.1257	1.950	0.756	c
C3-P-027	12.05	1.47E−14	40.2	0.1545	0.0784	4.574	2.174	c
C3-P-037	18.70	7.54E−15	51.4	0.3973	0.0784	4.094	1.761	c
C3-P-038	36.65	8.62E−16	59.6	0.4488	0.1257	2.451	0.641	c
C3-P-040	25.93	1.84E−15	47.6	0.4807	0.1257	3.105	0.837	c
RD109-GEO-01	29.60	1.10E−14	27.2	0.7137	0.0784	3.873	1.547	c
RD109-GEO-06	40.71	1.73E−15	32.1	0.6254	0.1257	1.215	0.667	c
RD109-GEO-14	25.48	3.33E−15	37.6	0.7505	0.2015	3.875	1.001	c
RD109-GEO-16	24.28	5.88E−15	39.5	0.7211	0.1257	3.281	1.363	c
RD109-P-01	21.50	3.90E−15	30.5	0.6033	0.0489	3.105	0.975	c
RD109-P-02	25.41	1.61E−15	44.6	0.5641	0.0784	2.180	0.758	c
RD109-P-03	25.60	7.52E−15	38.5	0.5911	0.3235	3.467	1.522	c
RD109-P-05	27.87	5.17E−15	46.6	0.6475	0.1257	2.816	1.388	c
RD109-P-06	22.11	1.11E−15	49.7	0.6646	0.0305	4.326	0.664	c
MP24S-P-001-1V	14.05	5.37E−15	44.0	0.2502	2.1507	7.959	1.375	c

(*Continued*)

Table 1 Continued

Sample name	S_{por} (1/μm)	k (in m²)	F	σ'' (mS/m)	τ_{pc} (s)	r_{dom} (μm)	r_{eff} (μm)	Reference†
MP24S-P-002-1V	3.23	6.12E−14	26.4	0.0343	0.5184	10.685	3.595	c
MP24S-P-002-2H	3.92	2.46E−13	30.8	0.0270	0.6523	10.685	7.786	c
MP24S-P-003-1V	19.08	7.82E−15	38.1	0.2036	3.4599	7.125	1.544	c
MP24S-P-003-2H	22.67	1.76E−14	49.8	0.1938	2.1507	7.125	2.648	c
MP24S-P-004-1V	2.28	3.26E−13	16.8	0.0834	0.5184	10.493	6.619	c
MP24S-P-004-2H	2.63	3.62E−13	20.4	0.0196	0.7330	10.493	7.686	c
MP24S-P-005-1V	78.45	1.72E−16	19.6	0.5543	1.3374	2.063	0.164	c
MP24S-P-006-1V	67.21	1.56E−15	16.5	0.3385	2.1507	4.096	0.454	c
MP24S-P-006-2H	86.03	6.43E−15	19.6	0.3262	2.1507	4.096	1.004	c
MP24S-P-007-1V	69.08	3.37E−16	23.4	0.1741	3.4599	11.089	0.251	c
MP24S-P-007-2H	62.95	6.23E−14	15.0	0.2526	2.1507	11.089	2.734	c
MP25S-P-001-1V	20.55	5.72E−15	20.8	0.2747	1.5010	2.688	0.976	c
MP25S-P-001-2H	22.22	5.87E−15	22.7	0.2796	1.1530	2.688	1.032	c
MP25S-P-002-1V	81.58	9.21E−17	45.4	0.1300	0.2280	0.315	0.183	c
MP25S-P-002-2H	73.55	1.78E−16	33.4	0.1521	0.2170	0.315	0.218	c
MP25S-P-003-1V	50.84	1.38E−14	38.4	0.1030	0.0780	0.418	2.059	c
MP25S-P-003-2H	52.08	4.01E−15	34.6	0.1545	0.2210	0.418	1.054	c
MP25S-P-004-1V	78.75	1.02E−15	27.4	0.2747	2.1507	2.082	0.473	c
MP25S-P-004-2H	81.35	7.83E−16	27.1	0.1447	1.3374	2.082	0.412	c
MP25S-P-006-1V	64.21	5.43E−15	14.6	0.3188	5.4881	8.888	0.796	c

†References: (a) Weller *et al.* (2015), (b) Weller *et al.* (2016), (c) Robinson *et al.* (2018).

nature of the surface of pores in sedimentary rocks not captured in the capillary bundle model (e.g. Pape, Riepe and Schopper 1987). The relatively high resolution of the nitrogen adsorption method captures this surface roughness. Unsurprisingly, r_{Spor} is less well correlated with r_{eff} than r_{dom}, although both geometrical length scales show a significant correlation with r_{eff}.

Geophysical length scale based on relaxation time τ

The relaxation time τ_{pc} is taken at the characteristic peak frequency f_{pc} in the plot of σ'' versus f representing the dominant dispersion. Equation (10) is used to determine the corresponding length scale $r_\tau = r_{\tau pc}$. Figure 2(a) shows the relationship between log of r_{eff} and the log of $r_{\tau pc}$. Assuming a linear relation between r_{eff} and $r_{\tau pc}$, the best-fitting relation is given by $r_{eff} = 0.700 r_{\tau pc}$. However, the coefficient of determination is negative ($R^2 = -0.086$). A negative value of the coefficient of determination indicates that the linear relation fits the data worse than a horizontal line corresponding to the mean value of $\log(r_{eff})$. Therefore, a reliable linear relation between r_{eff} and $r_{\tau pc}$ cannot be identified for the investigated set of sandstone samples. A similar result is found when a Debye decomposition procedure (e.g. Nordsiek and Weller 2008) is used to determine the mean relaxation time τ_{mean} (result not shown for brevity). The resulting coefficient of determination for a linear relation between r_{eff} and $r_\tau = r_{\tau mean}$ is $R^2 = -0.088$.

Geophysical length scales based on σ'' and $F\sigma''$

We first consider the length scale $r_{\sigma''}$ determined from the polarization magnitude assuming $\sigma'' \propto S_{por}$, in this case σ'' determined at 1 Hz. Figure 2(b) does not show any reliable linear relation between r_{eff} and $r_{\sigma''}$. The resulting coefficient of correlation is again negative ($R^2 = -0.017$). The underestimation of r_{eff} is consistent with the underestimation identified for r_{Spor}, an expected result if σ'' is linearly related to S_{por} via equation (6).

We now consider the length scale $r_{F\sigma''}$ determined from assuming $\sigma'' \propto S_{por}/F$. Figure 2(c) suggests that r_{eff} is better correlated with $r_{F\sigma''}$ relative to $r_{\sigma''}$. The coefficient of determination becomes positive ($R^2 = 0.242$) and confirms that a part of the scatter in r_{eff} can be explained by the linear relation $r_{eff} = 6.16 r_{F\sigma''}$.

Implications for k estimation

We use the linear relations identified by fitting the log of r_{eff}, which results from the known values of k and F using equation (2), to the logs of r_{dom}, r_{Spor}, $r_{\tau pc}$, $r_{\tau mean}$, $r_{\sigma''}$ and

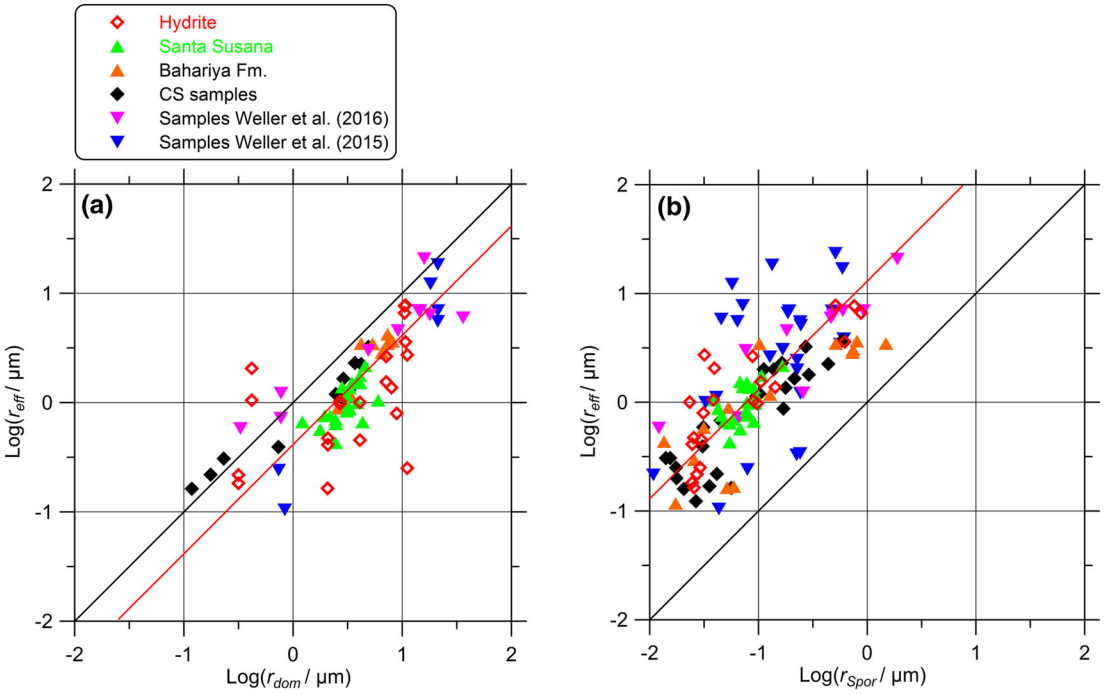

Figure 1 Effective hydraulic radius r_{eff} computed from equation (2) versus geometrical length scales (a) r_{dom}, and (b) r_{Spor}. Black lines represent the conditions (a) $r_{\text{eff}} = r_{\text{dom}}$, and (b) $r_{\text{eff}} = r_{\text{Spor}}$. Red lines represent the conditions (a) $\tilde{r}_{\text{eff}} = 0.414 r_{\text{dom}}$ ($R^2 = 0.528$) and (b) $\tilde{r}_{\text{eff}} = 13.0 r_{\text{Spor}}$ ($R^2 = 0.498$).

$r_{F\sigma''}$. We represent these proxies of the effective hydraulic radius as $\tilde{r}_{\text{eff}}$. The resulting fitting functions are summarized in Table 2. The coefficients of determination R^2 and the average absolute deviation d determined from the residuals of a cross-plot between the estimated permeability (k^*) using $\tilde{r}_{\text{eff}}$,

$$k^* = \frac{\tilde{r}_{\text{eff}}^2}{8F} \tag{16}$$

and the actual value of the measured permeability (k) on a logarithmic scale are included in Table 2. The smaller the value of d, the better the estimate of k using $\tilde{r}_{\text{eff}}$. If d reaches unity, the average deviation from the fitting line is one logarithmic decade or a factor of 10.

Figure 3 shows the cross-plots of k^* versus k when using r_{dom}, r_{Spor} and $r_{F\sigma''}$ as the proxy of effective hydraulic radius. The geometrical proxies of r_{eff} provide the best estimate of k. The geophysical proxy based on $r_{F\sigma''}$ results in a value of d that is larger than that obtained when using the geometrical proxies r_{Spor} and r_{dom}, but smaller when compared with the proxies based on the other geophysical length scales ($r_{\sigma''}$, $r_{\tau pc}$ and $r_{\tau\text{mean}}$) that provide very large values of d (approaching unity; Table 2) and do not show the expected 1:1 correlation between k^* and k. Plots of k^* versus k when using $r_{\sigma''}$, $r_{\tau pc}$ and $r_{\tau\text{mean}}$ are not shown for brevity.

Table 2 Summary of type of proxy effective hydraulic radius $\tilde{r}_{\text{eff}}$, the number of samples n, the linear relationships between $\tilde{r}_{\text{eff}}$ and the geometrical and geophysical length scales, the resulting coefficient of determination R^2, and the average absolute deviation (in log space) d calculated from a cross-plot of estimated permeability (k^*) using $\tilde{r}_{\text{eff}}$ and measured permeability k. Bold indicates relationships with a lower value of d and shown in Fig. 3

Type	n	Proxy of r_{eff}	R^2	$d^\dagger$
Geometrical (r_{dom})	78	$\tilde{r}_{\text{eff}} = 0.414 r_{\text{dom}}$	0.528	**0.476**
Geometrical (r_{Spor})	117	$\tilde{r}_{\text{eff}} = 13.0 r_{\text{Spor}}$	0.498	**0.578**
Geophysical ($r_{\tau pc}$)	102	$\tilde{r}_{\text{eff}} = 0.700 r_{\tau pc}$	−0.086	0.830
Geophysical ($r_{\tau\text{mean}}$)	119	$\tilde{r}_{\text{eff}} = 0.990 r_{\tau\text{mean}}$	−0.088	0.917
Geophysical ($r_{\sigma''}$)	119	$\tilde{r}_{\text{eff}} = 10.55 r_{\sigma''}$	−0.017	0.873
Geophysical ($r_{F\sigma''}$)	119	$\tilde{r}_{\text{eff}} = 6.16 r_{F\sigma''}$	0.242	**0.777**

$^\dagger d = \frac{1}{n}\sum_{i=1}^{n} |\log_{10}(k) - \log_{10}(k^*)|$

Empirical observations for the role of formation factor on permeability

It is informative to consider the empirical relationship between k and F. Equations (11)–(14) all predict a dependence of $k \propto F^{-1}$, whereas equation (15) predicts $k \propto F^{-3}$. The relationship between k and F is plotted in Fig. 4, where the least-squares fitting of a power-law results in $k \propto F^{-4.21}$, which is closest to the prediction given by equation (15).

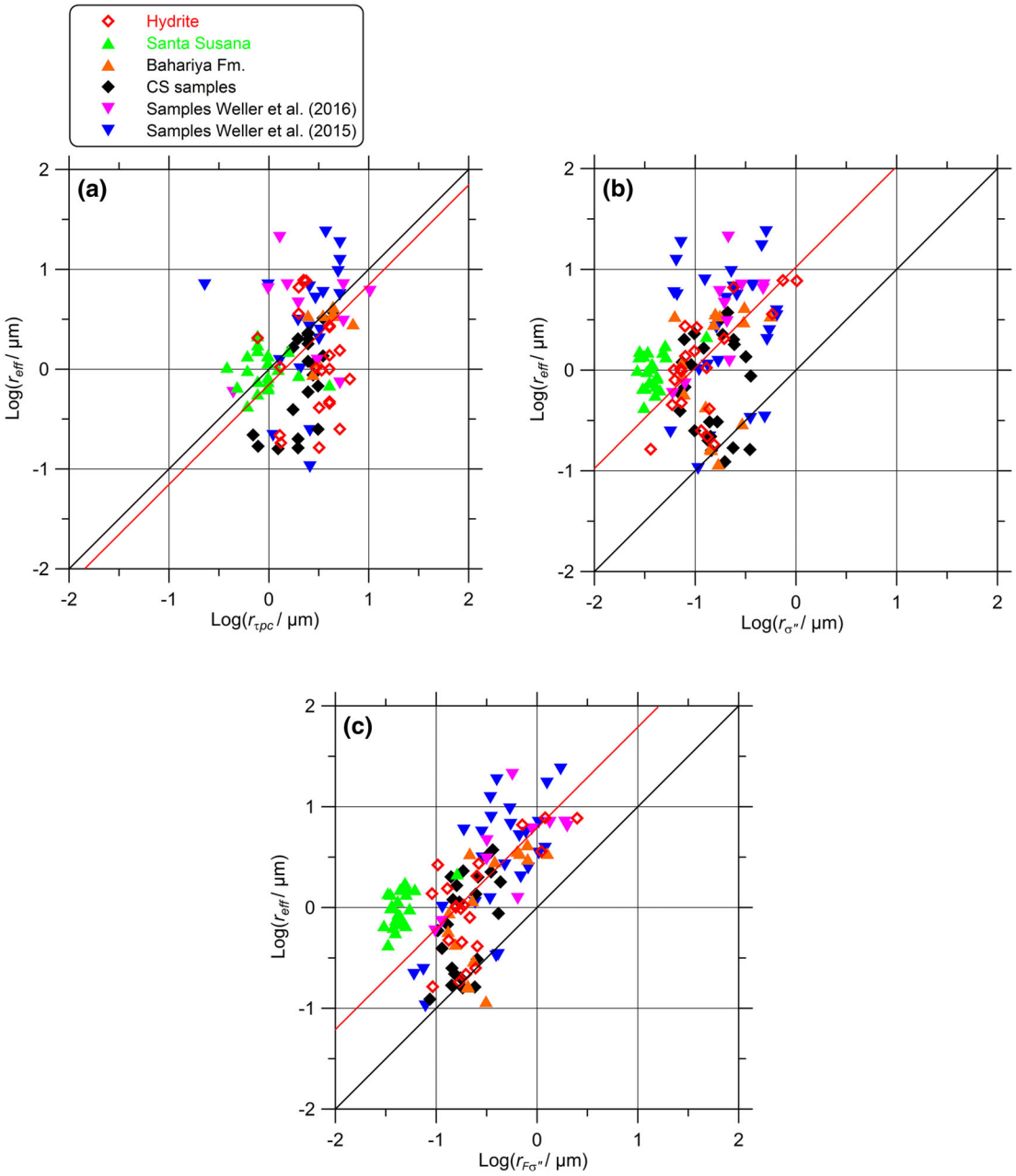

Figure 2 Effective hydraulic radius r_{eff} computed from equation (2) versus geophysical length scales (a) $r_{\tau pc}$, (b) $r_{\sigma''}$ and (c) $r_{F\sigma''}$. Black lines represent the conditions (a) $r_{\text{eff}} = r_{\tau pc}$, (b) $r_{\text{eff}} = r_{\sigma''}$ and (c) $r_{\text{eff}} = r_{F\sigma''}$. Red lines represent the conditions (a) $\tilde{r}_{\text{eff}} = 0.700 r_{\tau pc}$ ($R^2 = -0.086$), (b) $\tilde{r}_{\text{eff}} = 10.55 r_{\sigma''}$ ($R^2 = -0.017$) and (c) $\tilde{r}_{\text{eff}} = 6.16 r_{F\sigma''}$ ($R^2 = 0.242$).

Empirical observations for the role of formation factor on the specific chargeability

Accepting that specific polarizability should represent the effect of the fluid chemistry on polarization strength independent of pore geometry, then the revised version of the specific polarizability c_q should not show a significant relationship with either the porosity ϕ or the formation factor F. Figure 5 confirms this to be the case, with c_q versus ϕ plotted in Fig. 5(a) and c_q versus F plotted in Fig. 5(b). Although the two graphs indicate a variation of the specific polarizability c_q over two orders of magnitude, a dependence on both porosity and formation factor is not observed.

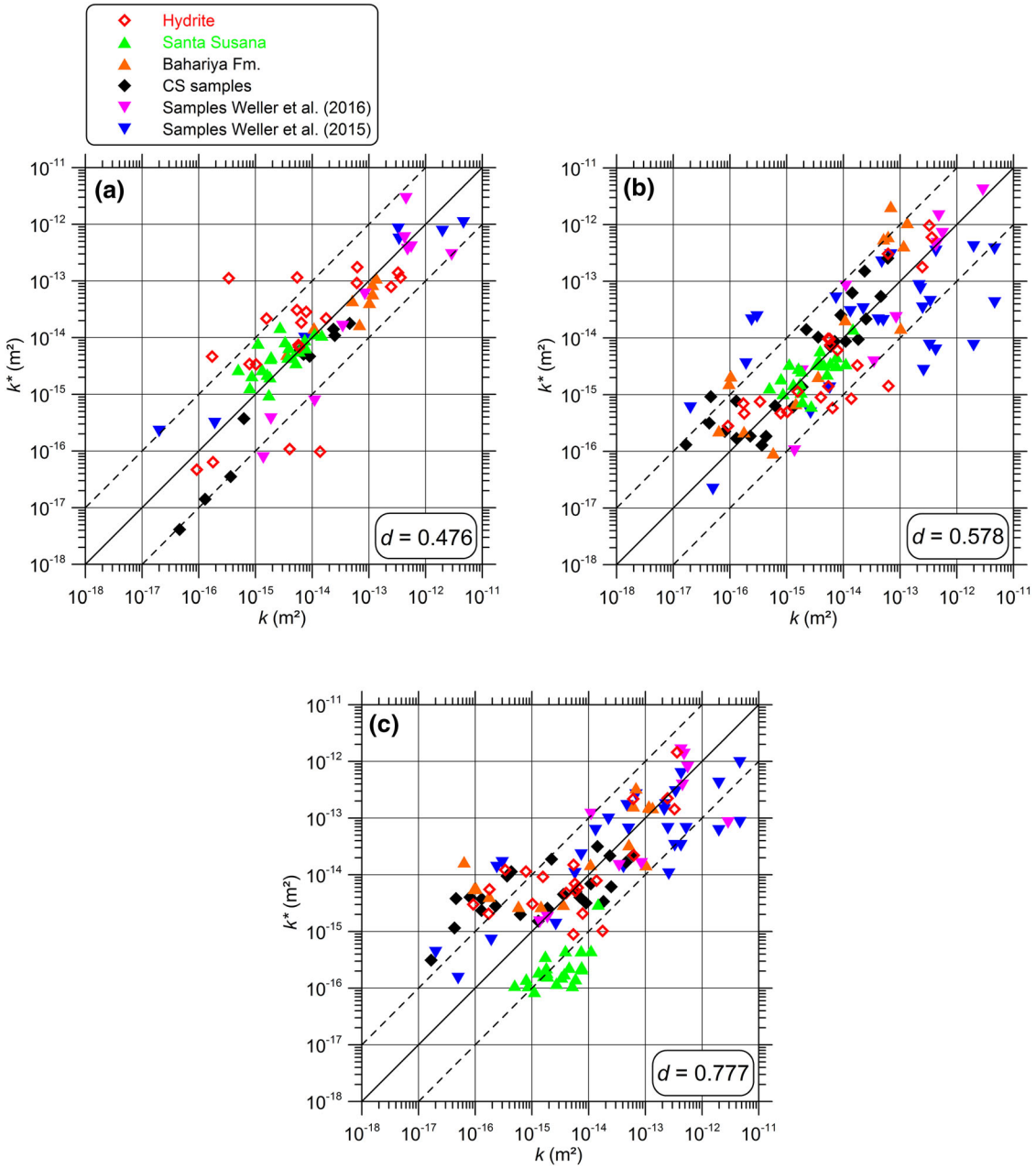

Figure 3 Permeability estimates (k^*) from $\tilde{r}_{\text{eff}}$ versus measured permeability (k) (a) for $\tilde{r}_{\text{eff}} = 0.414 r_{\text{dom}}$, (b) for $\tilde{r}_{\text{eff}} = 13.0 r_{\text{Spor}}$ and (c) for $\tilde{r}_{\text{eff}} = 6.16 r_{F\sigma''}$. In each case, the solid line defines the condition $k^* = k$ and the dashed lines indicate ± one order of magnitude of variation. The parameter $d = \frac{1}{n}\sum_{i=1}^{n} |\log_{10}(k) - \log_{10}(k^*)|$ is shown on each graph.

DISCUSSION

The fact that the geometrical parameter controlling measures of the polarization strength (σ'' or normalized chargeability m_n) should be S_{por}/F has been recognized for decades (e.g. Börner 1992). Weller and Slater (2012) showed that this proportionality is consistent with theoretical models for the induced-polarization effect based on Stern layer polarization (Leroy *et al.* 2008; Revil and Florsch 2010; Revil and Skold 2011) and diffuse layer polarization (Rink and Schopper 1974; Börner 1992). Börner *et al.* (1996) proposed the simplification to $\sigma'' \propto S_{\text{por}}$ based on the specific conditions of 'constant water composition and slightly varying formation

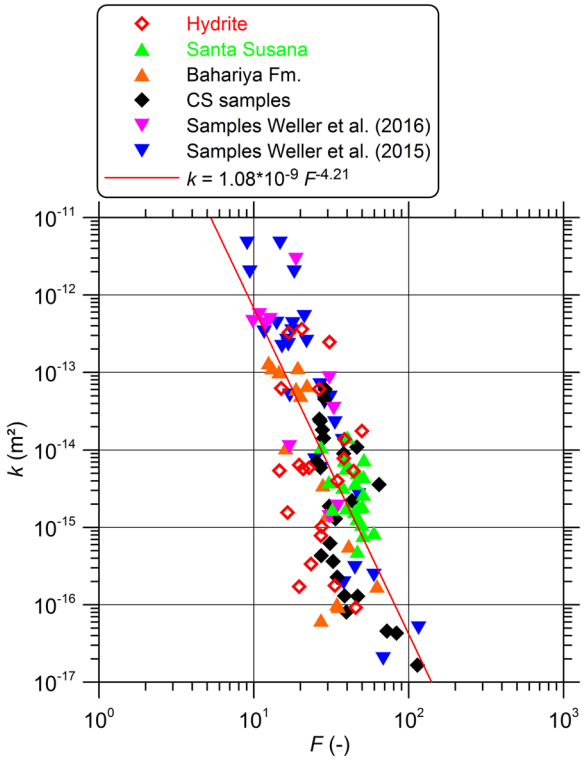

Figure 4 Measured permeability plotted versus measured formation factor. The solid red line defines the best-fitting power-law relation with an exponent equal to −4.21 and a coefficient of determination $R^2 = 0.533$.

factor'. Weller *et al.* (2010b) showed that this simplification is reasonable for a database of 114 predominantly sandstone and unconsolidated sediment samples originating from multiple independent data sets. They found a strong single linear empirical model describes the relationship between σ'' and S_{por} with the fitting constant c_p equal to 10^{-11} S. Niu *et al.* (2016) present experimental evidence for $\sigma'' \propto S_{por}$ failing to hold in tight clayey rocks characterized by relatively large values of F and S_{por}. They demonstrated that these samples are better described by $\sigma'' \propto S_{por}/F$, providing a theoretical derivation of this relationship by averaging the surface conductance over the pore volume. Niu *et al.* (2016) also pointed out that the $\sigma'' \propto S_{por}$ relation holds well for higher porosity materials such as sandstones.

Accepting that $\sigma'' \propto S_{por}/F$ results in a new geophysical length scale that can be substituted into equation (1) to yield a predictive formula for estimating permeability that has $k \propto (\sigma'')^{-2}$ and $k \propto (F)^{-3}$. In contrast, permeability equations using the other geophysical length scales defined in this study all predict $k \propto (F)^{-1}$. Revil, Kessouri and Torres-Verdín (2014) point out that a mechanistic model for k estimation from IP data in granular media (Revil and Florsch 2010) results in $k \propto (F)^{-3}$. Furthermore, laboratory observations using large databases support a much lower value for the exponent on F than −1, with empirically derived coefficients being closer to the value of −3. Thus, substitution of the geophysical

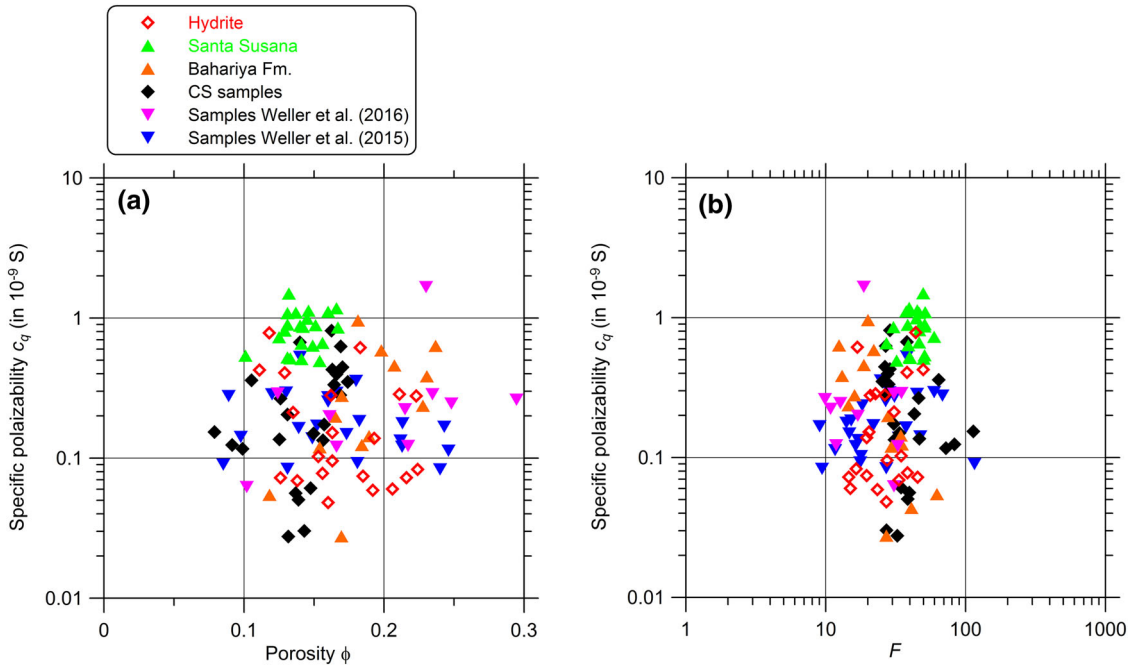

Figure 5 Evidence that the specific polarizability c_q is independent of the pore geometry (a) c_q versus porosity (b) c_q versus formation factor (F).

length scale $r_{F\sigma''}$ into the Hagen–Poiseuille equation results in a permeability prediction equation with a dependence on F that is consistent with other recent theoretical treatments of the IP effect as well as with empirical observations. This new permeability equation results in estimates of permeability that are better compared with other models based on IP parameters but do not reach the quality of those obtained with the geometric length scales (r_{dom}, r_{Spor}).

Equation (8) summarizes the fact that three geometrical factors control σ'', that is, control the surface conductivity. These factors are S_{por} (or the pore radius), the total porosity (ϕ) and the tortuosity ($T = F\phi$) of the pore space. All prior IP observations on specific types of samples are consistent with the proportionalities identified in equation (8). The finding $\sigma'' \propto S_{\mathrm{por}}$ reported by Weller *et al.* (2010b) follows for a limited range in F (Börner *et al.* 1996). The finding $\sigma'' \propto S_m$, where S_m is the specific surface area normalized to the mass of the sample, reported by Revil (2012) is expected for samples characterized by small porosities ($\phi << 1$, $(1-\phi)$ close to 1). Regarding the tortuosity, the finding $\sigma'' \propto 1/T \propto 1/\phi F$ (e.g. Revil 2013) can be expected when samples are characterized by similar values of S_m, such as the Fontainebleau sandstone (Revil *et al.* 2014). In the case of our study, samples are from different formations resulting in a wide range of F, T, S_{por} (or S_m). Consequently, the effect of all three geometrical factors is captured in our database.

The use of 1 Hz as a reference frequency for the imaginary conductivity has its origins in the work of Börner and Schön (1991) and is based on a constant phase angle model approximation for sandstones. Weller *et al.* (2010b) integrated the data from Börner and Schön (1991) into an extensive database that compiled samples from nine independent studies. They continued the use of 1 Hz as a reference frequency as it is located central to most SIP spectra and can thus be regarded as a good reference when a single frequency measurement is made. They also reported values of σ'' at 1 Hz for a saturating fluid salinity of 100 mS/m in order to remove variations in specific polarizability between samples. We followed the same approach in this work. However, we also computed normalized chargeability for each sample based on a Debye decomposition procedure that can be considered a global estimate of the polarization strength over the entire frequency range. The results, not shown for brevity, were consistent with those found for σ'' at 1 Hz, and did not yield a significant improvement in prediction of r_{eff} or k.

Incorporating the role of F on the imaginary conductivity when dealing with a wide range of formation types requires a modification to the specific polarizability concept introduced by Weller *et al.* (2010b, 2011). The specific polarizability should be independent of the pore geometry and thereby only represent the effects of the interfacial chemistry (largely controlled by the pore fluid chemistry and the mineralogy) on imaginary conductivity. The original definition, $c_p = \sigma''/S_{\mathrm{por}}$ (Weller *et al.* 2011), neglects the role of the formation factor discussed here. The revised definition $c_q = F\sigma''/S_{\mathrm{por}}$ should be independent of the pore geometry. Figure 5 confirms that this is indeed the case and that c_q is the correct representation of the effect of the interfacial chemistry on polarizability required when dealing with a wide variety of samples with large variability in F and ϕ. The simplification to c_p is appropriate when dealing with a limited range of formation types, for example, the unconsolidated sediments and sandstones reported in the extensive database of Weller *et al.* (2010b).

Previous studies have argued that the original specific polarizability c_p may vary over a relatively narrow range (Weller *et al.* 2010b, 2015; Robinson *et al.* 2018), with positive implications for estimating pore geometric parameters and, by extension, permeability from induced-polarization measurements, for example, using empirically derived relationships. In contrast, we find that individual values of c_q vary over almost two orders of magnitude for our database. Figure 5 shows that, with the exception of the CS samples, samples from specific formations cluster together around a limited range of c_q variation, consistent with the concept that c_q is in large part controlled by the rock mineralogy, which varies substantially between the different formations. Thus, empirically derived relationships between σ'' and pore geometric parameters and, by extension, permeability should not be expected to hold outside of the range of formation/mineralogy they are calibrated on. The limited range in c_p identified by previous authors is a logical result of the fact that the databases used in these previous studies represented a limited range of material types.

Our study has some important implications for the long-explored effort to estimate permeability from induced-polarization measurements. First, we find that the geophysical length scale associated with measures of the relaxation time does not appear to be a reliable indicator of permeability. Weller *et al.* (2016) discussed the challenges of estimating a proxy effective hydraulic radius from the time constant that result from variations in the diffusion coefficient. This increasingly appears to be a fundamental limitation of the approach, especially when considering a broad range of formation types where variations in diffusion coefficient are likely to be accentuated. Kruschwitz *et al.* (2010) identified five orders of magnitude in variation in the effective diffusion coefficients, observing a strong correlation between pore throat diameter and

effective diffusion coefficient. Weller *et al.* (2016) reported six orders of magnitude of variation in an apparent diffusion coefficient using equation (10) and assuming $r_t = r_{\text{eff}}$.

However, our study also highlights an inherent limitation of the approach to estimating permeability based on an effective hydraulic radius determined from a measure of the polarization magnitude, that is, imaginary conductivity or normalized chargeability. Börner *et al.* (1996) first introduced the concept of combining a geophysical proxy of r_{eff} with the formation factor in a permeability estimation model. In doing so, they implicitly recognized the need to assume a limited range in the formation factor to produce a direct linear relationship between σ'' and S_{por}, that is, that the simplification $\sigma'' \propto S_{\text{por}}/F$ to $\sigma'' \propto S_{\text{por}}$ can be assumed as valid. This simplification is critical as it allows the IP measurement to isolate the effect of the pore radius from the tortuosity of the pore space, as needed to reliably estimate permeability. The success of this electrical approach to permeability estimation has been documented in numerous studies where samples are characterized by a limited range in the formation factor. The approach has proven particularly effective in unconsolidated sediments, where formation factors are low and limited to a narrow range (Slater and Lesmes 2002; Maurya *et al.* 2018). When the role of F on σ'' becomes significant, IP measurements become ambiguous as they then depend both on the pore radius, along with the tortuosity and porosity of the porous network. It is interesting to note that early efforts to estimate permeability from electrical resistivity measurements alone were thwarted by the fact that the real part of the conductivity is controlled by both electrolytic conduction (porosity, formation factor) and surface conduction (surface area, pore size; e.g. Purvance and Andricevic 2000). The opportunity identified by Börner *et al.* (1996) was that IP overcame this limitation by providing a direct measurement of the surface area (or pore size). Unfortunately, this simplification can only be expected to hold over a limited range of formation types such that formation factor does not exert a strong control on the imaginary conductivity.

This study focused on a comprehensive database of isotropic sandstone samples. A similar database is not available for carbonates or magmatic rocks. Future studies should verify whether the presented findings are transferable to measurements on other rock types. In the presence of anisotropy, permeability prediction will be complicated by the directional dependence of the IP parameters and the formation factor, which can be investigated by measurements on the samples in different directions (e.g. Weller, Nordsiek and Debschütz 2010a). Geometric parameters, such as specific internal surface and the pore throat radius, do not consider anisotropy. Hence, it is possible that the geophysical length scales will have advantages over the geometric length scales for permeability prediction in the presence of anisotropy.

CONCLUSIONS

The definition of an effective hydraulic radius determined from induced-polarization measurements must consider the control of the electrical formation factor on the polarization magnitude when samples cover a wide range of formation types and a correspondingly wide range in variation in the electrical formation factor. Recognizing that the imaginary conductivity should be proportional to the pore volume normalized surface area divided by the formation factor results in a new geophysical length scale and a permeability prediction equation where permeability is proportional to F^{-3}. This proportionality is consistent with some mechanistic models for the polarization of granular media and also consistent with a number of experimental data sets made on consolidated rocks. Furthermore, this new geophysical length scale results in an improved prediction of permeability relative to other permeability prediction equations based on geophysical length scales where permeability is proportional to F^{-1}. However, with this equation, the quality of permeability estimates does not reach the level of those obtained when a geometrical proxy of the effective hydraulic radius defined from the pore volume normalized surface area is used. The joint dependence of induced-polarization measurements on both the pore radius and the tortuosity and porosity of the interconnected pore network is a limitation to the widely explored use of induced-polarization measurements to isolate surface properties from volumetric properties of the interconnected pore network.

ACKNOWLEDGEMENTS

We thank Ms. Haoman Li for her assistance in compiling the database. The constructive comments received from the reviewers, particularly Niels Grobbe, significantly improved the manuscript.

REFERENCES

Börner F. 1992. Complex conductivity measurements of reservoir properties. In: *Advances in Core Evaluation III (Reservoir Management)* (ed P. F. Worthington), pp. 359–386. Gordon and Breach Science Publishers, London, Reading.

Börner F.D. and Schön, J.H. 1991. A relation between the quadrature component of electrical conductivity and the specific surface area of sedimentary rocks. *The Log Analyst* **32**, 612–613.

Börner F.D., Schopper J.R. and Weller, A. 1996. Evaluation of transport and storage properties in the soil and groundwater zone from induced polarization measurements. *Geophysical Prospecting* **44**, 583–601.

Breede K. 2006. *SIP-Messungen an Sandsteinen*. Diplomarbeit, Technische Universität Clausthal.

Brunauer S., Emmett P. and Teller E. 1938. Adsorption of gases on multi-molecular layers. *Journal of the American Chemical Society* **60**, 309–319.

Katz A.J. and Thompson A.H. 1987. Prediction of rock electrical-conductivity from mercury injection measurements. *Journal of Geophysical Research-Solid Earth and Planets* **92**, 599–607.

Kruschwitz S., Binley A., Lesmes D. and Elshenawy A. 2010. Textural controls on low-frequency electrical spectra of porous media. *Geophysics* **75**, WA113–WA123.

Leroy P., Revil A., Kemna A., Cosenza P. and Ghorbani A. 2008. Complex conductivity of water-saturated packs of glass beads. *Journal of Colloid and Interface Science* **321**, 103–117.

Lesmes D.P. and Frye K.M. 2001. The influence of pore fluid chemistry on the complex conductivity and induced-polarization response of Berea sandstone. *Journal of Geophysical Research* **106**, 4079–4090.

Maurya P.K., Balbarini N., Møller I., Rønde V., Christiansen A.V., Bjerg P.L., et al. 2018. Subsurface imaging of water electrical conductivity, hydraulic permeability and lithology at contaminated sites by induced polarization. *Geophysical Journal International* **213**, 770–785.

Niu Q., Prasad M., Revil A. and Saidian M. 2016. Textural control on the quadrature conductivity of porous media. *Geophysics* **81**, E297–E309.

Nordsiek S. and Weller A. 2008. A new approach to fitting induced-polarization spectra. *Geophysics* **73**, F235–F245.

Öner Ü., Weller A., Sattler C.-D. and Kassab M.A. 2016. Petrographic and petrophysical investigation of carbonate samples (Upper Cretaceous) from Tushka Area (Egypt) with special focus on the effective pore radius. *Arabian Journal of Geosciences* **9**, 229.

Pape H., Clauser C. and Iffland J. 1999. Permeability prediction based on fractal pore-space geometry. *Geophysics* **64**, 1447–1460.

Pape H., Riepe L. and Schopper J.R. 1987. Theory of self-similar network structures in sedimentary and igneous rocks and their investigation with microscopical methods. *Microscopy* **148**, 121–147.

Purvance D.T. and Andricevic R. 2000. Geoelectric characterization of the hydraulic conductivity field and its spatial structure at variable scales. *Water Resources Research* **36**, 2915–2924.

Revil A. 2012. Spectral induced polarization of shaly sands: influence of the electrical double layer. *Water Resources Research* **48**, W02517.

Revil A. 2013. On charge accumulation in heterogeneous porous rocks under the influence of an external electric field. *Geophysics* **78**, D271–D291.

Revil A., Binley A., Mejus L. and Kessouri P. 2015. Predicting permeability from the characteristic relaxation time and intrinsic formation factor of complex conductivity spectra. *Water Resources Research* **51**, 6672–6700.

Revil A. and Florsch N. 2010. Determination of permeability from spectral induced polarization in granular media. *Geophysical Journal International* **181**, 1480–1498.

Revil A., Kessouri P. and Torres-Verdín C. 2014. Electrical conductivity, induced polarization, and permeability of the Fontainebleau sandstone. *Geophysics* **79**, D301–D318.

Revil A., Koch K. and Holliger K. 2012. Is it the grain size or the characteristic pore size that controls the induced polarization relaxation time of clean sands and sandstones? *Water Resources Research* **48**, 1–7.

Revil A. and Skold M. 2011. Salinity dependence of spectral induced polarization in sands and sandstones. *Geophysical Journal International* **187**, 813–824.

Rink M. and Schopper J.R. 1974. Interface conductivity and its implications to electric logging. In *SPWLA 15th Annual Logging Symposium*, McAllen, Texas, paper J.

Robinson J., Slater L., Weller A., Keating K., Robinson, T., Rose, C. et al. 2018. On permeability prediction from complex conductivity measurements using polarization magnitude and relaxation time. *Water Resources Research* **54**, 3436–3452.

Schröder H. 2008. *SIP-Messungen an mit unterschiedlichen Salzlösungen gesättigten Sandsteinen*. Diplomarbeit, Technische Universität Clausthal.

Scott J.B.T. and Barker R.D. 2003. Determining pore-throat size in Permo-Triassic sandstones from low-frequency electrical spectroscopy. *Geophysical Research Letters* **30**, 1450.

Slater L. and Lesmes D. 2002. IP interpretation in environmental investigations. *Geophysics* **67**, 77–88.

Weller A., Breede K., Slater L. and Nordsiek S. 2011. Effect of changing water salinity on complex conductivity spectra of sandstones. *Geophysics* **76**, F315–F327.

Weller A., Nordsiek, S. and Debschütz, W. 2010a. Estimating permeability of sandstone samples by nuclear magnetic resonance and spectral-induced polarization. *Geophysics* **75**, E215–E226.

Weller A. and Slater L. 2012. Salinity dependence of complex conductivity of unconsolidated and consolidated materials: comparisons with electrical double layer models. *Geophysics* **77**, 185–198.

Weller A., Slater L., Binley A., Nordsiek S. and Xu S. 2015. Permeability prediction based on induced polarization: insights from measurements on sandstone and unconsolidated samples spanning a wide permeability range. *Geophysics* **80**, D161–D173.

Weller A., Slater L. and Nordsiek S. 2013. On the relationship between induced polarization and surface conductivity: Implications for petrophysical interpretation of electrical measurements. *Geophysics* **78**, D315–D325.

Weller A., Slater L., Nordsiek S. and Ntarlagiannis D. 2010b. On the estimation of specific surface per unit pore volume from induced polarization: a robust empirical relation fits multiple data sets. *Geophysics* **75**, WA105–WA112.

Weller A., Zhang Z., Slater L., Kruschwitz S. and Halisch M. 2016. Induced polarization and pore radius – a discussion. *Geophysics* **81**, D519–D526.

Zhang Z. and Weller A. 2014. Fractal dimension of pore space geometry of an Eocene sandstone formation. *Geophysics* **79**, D377–D387.

